



Thermal and electrical conductivity of solid iron and iron–silicon mixtures at Earth's core conditions



Monica Pozzo^{a,*}, Chris Davies^b, David Gubbins^{b,c}, Dario Alfè^a

^a Department of Earth Sciences, Department of Physics and Astronomy, London Centre for Nanotechnology and Thomas Young Centre@UCL, University College London, Gower Street, London WC1E 6BT, United Kingdom

^b School of Earth and Environment, University of Leeds, Leeds LS2 9JT, UK

^c Institute of Geophysics and Planetary Physics, Scripps Institution of Oceanography, University of California at San Diego, 9500 Gilman Drive no. 0225, La Jolla, CA 92093-0225, USA

ARTICLE INFO

Article history:

Received 27 June 2013

Received in revised form 5 December 2013

Accepted 23 February 2014

Available online xxxx

Editor: C. Sotin

Keywords:

inner core
conductivity
geodynamo
core convection
first principles
mineral physics

ABSTRACT

We report on the thermal and electrical conductivities of solid iron and iron–silicon mixtures ($\text{Fe}_{0.92}\text{Si}_{0.08}$ and $\text{Fe}_{0.93}\text{Si}_{0.07}$), representative of the composition of the Earth's solid inner core at the relevant pressure–temperature conditions, obtained from density functional theory calculations with the Kubo–Greenwood formulation. We find thermal conductivities $k = 232$ (237) $\text{W m}^{-1} \text{K}^{-1}$, and electrical conductivities $\sigma = 1.5$ (1.6) $\times 10^6$ $\Omega^{-1} \text{m}^{-1}$ at the top of the inner core (centre of the Earth). These values are respectively about 45–56% and 18–25% higher than the corresponding conductivities in the liquid outer core. The higher conductivities are due to the solid structure and to the lower concentration of light impurities. These values are much higher than those in use for previous inner core studies, k by a factor of four and σ by a factor of three. The high thermal conductivity means that heat leaks out by conduction almost as quickly as the inner core forms, making thermal convection unlikely. The high electrical conductivity increases the magnetic decay time of the inner core by a factor of more than three, lengthening the magnetic diffusion time to 10 kyr and making it more likely that the inner core stabilises the geodynamo and reduces the frequency of reversals.

© 2014 Elsevier B.V. All rights reserved.

1. Introduction

This paper follows previous articles (Pozzo et al., 2012, 2013), in which we reported on the electrical and thermal conductivities of liquid iron and iron mixtures at Earth's outer core conditions computed with density functional theory (DFT) and the Kubo–Greenwood (KG) relation. Here we extend those results to the Earth's solid inner core. The conductivities are important in determining the fundamental time scales for diffusion of heat and magnetic field within the inner core.

The study of the inner core is key to understanding the thermal and dynamic processes of the Earth. It formed, and continues to grow, as a result of the Earth's slow cooling, a process central to powering the geodynamo through the release of latent heat and compositional buoyancy resulting from fractionation of light elements into the liquid as it freezes. The inner core is seismically anisotropic (Tromp, 2001) and may contain distinct layers (Ishii and Dziewonski, 2002). Shear flow is re-

quired to align crystals and form the anisotropy and solid convection has been invoked as one possible mechanism (Jeanloz and Wenk, 1988). The layering could be a result of thermal convection switching on and shutting off as the temperature gradient rises above, or falls below, the adiabatic gradient (Yukutake, 1998; Buffett, 2009). The thermal conductivity is vital for determining whether the inner core has ever undergone convection.

A conducting inner core has been shown to determine the stability and frequency of polarity reversals in several numerical geodynamo models (Hollerbach and Jones, 1993; Glatzmaier and Roberts, 1995). The geomagnetic field reverses on average a few times in a million years while excursions, events where the polarity reverses briefly but fails to establish the reversed state, are about ten times more frequent (Laj and Channel, 2007). Gubbins (1999) suggested that excursions are a result of the outer core field reversing for too short a time to reverse the field in the inner core. The number of excursions compared to the number of reversals would then depend on the ratio of the magnetic diffusion timescale in the outer and inner cores. More recent dynamo simulations have produced conflicting results, with some showing no effect of conduction in the inner core (Wicht, 2002) and

* Corresponding author.

E-mail address: m.pozzo@ucl.ac.uk (M. Pozzo).

others a clear change (Dharmaraj and Stanley, 2012). The different results appear to depend on the different parameters and boundary conditions used in the models (Dharmaraj and Stanley, 2012). In any case, the electrical conductivity is crucial for determining the timescale for magnetic changes in the inner core and the ratio of conductivities between the two cores may be important in determining the degree of stability the inner core imparts on the geodynamo.

The electrical (σ) and thermal (k) conductivities of solid iron have been measured by Gomi et al. (2010) and Konôpková et al. (2011) who found σ of about $10 \times 10^6 \Omega^{-1} \text{m}^{-1}$ at room temperature and up to a pressure of 65 GPa, and k of about $30 \text{ W m}^{-1} \text{K}^{-1}$ at 2000 K and up to pressure 70 GPa, respectively. More recently, Deng et al. (2013) measured the electrical resistivity of iron up to 15 GPa and 2200 K. They found a value for the electrical conductivity of $2.2 \times 10^6 \Omega^{-1} \text{m}^{-1}$ at 15 GPa and 1500 K, and a value for the thermal conductivity of about $100 \text{ W m}^{-1} \text{K}^{-1}$ at 7 GPa and in the temperature range 600–1300 K. These pressure–temperature conditions are far from those found in the Earth’s core. Gomi et al. (2013) measured the electrical resistivity of a solid iron alloy (4 at.% Si) at high-pressure and 300 K finding an electrical conductivity of about $2.5 \times 10^6 \Omega^{-1} \text{m}^{-1}$ at 70 GPa. To extrapolate their results to core temperatures they combined their measurements with the saturation resistivity model, which says that the resistivity of a material stops increasing with temperature once the mean free path of the electrons becomes of the order of the interatomic distance (Gunnarsson et al., 2003). Within this model, their extrapolated values for the electrical and thermal conductivity of $\text{Fe}_{78}\text{Si}_{22}$ at $T = 3750$ (4971) K and $P = 135$ (330) GPa, representative of inner core (outer core) boundary conditions, were 0.98 (1.22) $\times 10^6 \Omega^{-1} \text{m}^{-1}$ and 90 (148) $\text{W m}^{-1} \text{K}^{-1}$, respectively. On the theoretical side conductivities of solid iron were calculated by Sha and Cohen (2011) using the low-order variational approximation. They found values of 1.1 – $1.8 \times 10^6 \Omega^{-1} \text{m}^{-1}$ and 160 – $162 \text{ W m}^{-1} \text{K}^{-1}$ for σ and k respectively. This approximation is generally valid up to $T = 2\Theta_{\text{tr}}$, where Θ_{tr} is the temperature corresponding to the average transport frequency, which is estimated to be about 633 K for hcp Fe at 330 GPa. Nevertheless, these results point to relatively high conductivities for the Earth’s inner core.

The Earth’s solid core is slightly less dense than pure iron under the same pressure–temperature conditions, and therefore must contain some small fraction of light impurities (Poirier, 1994). These light impurities partition at the inner core boundary (ICB) in a way that is governed by their chemical potentials in the solid and the liquid phases. First principles calculations of the chemical potentials of silicon, sulphur and oxygen established that oxygen partitions almost completely into the liquid, and therefore the composition of the solid must be based on a silicon/sulphur mixture (Alfè et al., 2007). This partitioning is also responsible for a decrease of the temperature of the mixture compared to the melting temperature of pure iron.

Here we compute the conductivities of pure solid iron at pressures close to that at the ICB, $p = 329$ GPa, and to the centre of the Earth, $p = 364$ GPa, at the DFT melting temperature of pure iron $T_{\text{m}} = 6350$ K (Alfè et al., 2002; Alfè, 2009; Anzellini et al., 2013). We have also computed the conductivities of $\text{Fe}_{0.92}\text{Si}_{0.08}$ and $\text{Fe}_{0.93}\text{Si}_{0.07}$ mixtures. These two mixtures are in equilibrium with liquid mixtures $\text{Fe}_{0.82}\text{Si}_{0.10}\text{O}_{0.08}$ and $\text{Fe}_{0.79}\text{Si}_{0.08}\text{O}_{0.13}$, and correspond to ICB solid–liquid coexisting temperatures of 5700 and 5500 K, respectively (Alfè et al., 2007; Pozzo et al., 2012, 2013).

This paper is organised as follows. In Section 2 we describe the techniques used in the calculations. The results for the thermal and electrical conductivities for pure solid iron and two iron–silicon mixtures are presented in Section 3. The implications of the results are discussed in Section 4. Conclusions follow in Section 5.

2. Techniques

The DFT technical details used in this work are identical to those used in (Alfè et al., 2012; Pozzo et al., 2012, 2013). First principles simulations were performed using the VASP code (Kresse and Furthmüller, 1996), with the projector augmented wave (PAW) method (Blöchl, 1994; Kresse and Joubert, 1999) and the Perdew–Wang (PW91) functional (Wang and Perdew, 1991; Perdew et al., 1992). For the molecular dynamics calculations, the PAW potential for oxygen, silicon and iron have the $2s^2 2p^4$, $3s^2 3p^2$ and $3p^6 4s^1 3d^7$ valence electronic configurations respectively, and the core radii were 0.79, 0.8 and 1.16 Å. Earlier tests (Pozzo et al., 2012, 2013) showed that the conductivities of pure iron and those of the mixtures are unaffected by using an iron PAW potential with the $4s^1 3d^7$ valence configuration instead, and so to compute the conductivities this is what we used. Single particle orbitals were expanded in plane-waves with a cutoff of 380 eV. Electronic levels were occupied according to Fermi–Dirac statistics, with an electronic temperature corresponding to the temperature of the system. An efficient extrapolation of the charge density was used to speed up the *ab initio* molecular dynamics simulations (Alfè, 1999), which were performed on 288-atom cells and sampling the Brillouin zone (BZ) with the Γ point only. The temperature was controlled with an Andersen thermostat (Andersen, 1980) and the time step was set to 1 fs. We ran simulations for typically 8–13 ps, from which we discarded the first ps to allow for equilibration. We then extracted more than 20 configurations (more precisely, 40 for pure solid iron and 24 for the solid iron–silicon mixtures) separated in time by 0.25 ps, which guarantees that they are statistically uncorrelated, and calculated the conductivities on these ionic configurations using the KG formula, as implemented in VASP by Desjarlais et al. (2002). We used two \mathbf{k} -points in the BZ, which guarantees convergence of the conductivities to better than 1.5%. For specific details of the calculations we refer to Pozzo et al. (2013).

3. Results

3.1. Iron

We begin our discussion by presenting the electrical and thermal conductivities of pure iron. We computed them at the three different temperatures, 6350, 5700 and 5500 K, and two pressures close to ICB pressure and the pressure at the center of the Earth. Results are displayed in Fig. 1 and also reported in Table 1. The conductivities of pure iron at Earth’s outer core conditions have been reported before (Pozzo et al., 2012, 2013), but for convenience we re-plot them here on the same figure. The temperature profiles are displayed in the bottom panel of Fig. 1: they are constant in the inner core and adiabatic in the outer core. The values for the electrical and thermal conductivities in pure solid iron are in the range 1.76 – $1.97 \times 10^6 \Omega^{-1} \text{m}^{-1}$ and 286 – $330 \text{ W m}^{-1} \text{K}^{-1}$, respectively, with the low/high values corresponding to ICB/Earth’s centre pressure–temperature conditions. The electrical conductivities increase by ~ 13 – 20% going from the liquid to the solid, with the largest increase corresponding to the lowest temperature. This is expected as the electronic mean free path increases with increasing order. A solid is more ordered than a liquid, and order increases with decreasing temperature.

In metals the thermal conductivity is related to the electrical conductivity via the empirical Wiedemann–Franz (WF) law (Wiedemann and Franz, 1853): $k = T\sigma L$, where L is a constant of proportionality known as the Lorenz parameter, equal to $2.44 \times 10^{-8} \text{ W}\Omega\text{K}^{-2}$ in the ideal case of a free electron metal. The linear increase of k with temperature is due to the linear increase of the electronic specific heat with temperature: hotter electrons

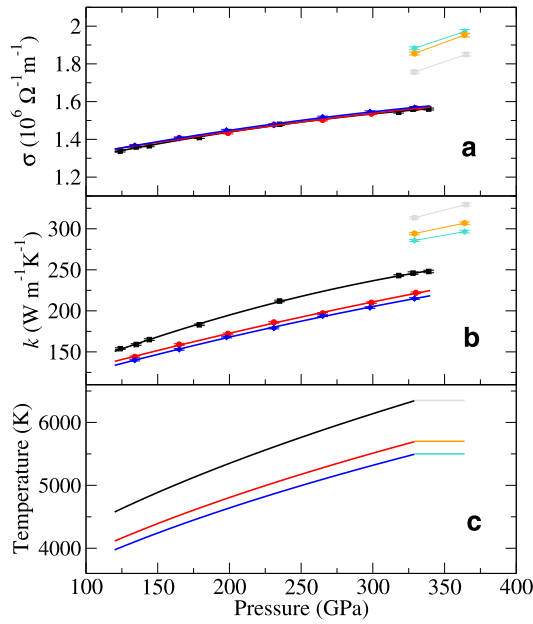


Fig. 1. Electrical conductivity, σ (a), and electronic component of the thermal conductivity, k (b), of pure iron corresponding to the three outer/inner core adiabatic profiles displayed in (c). Black/grey lines: $T_{\text{ICB}} = 6350$ K; red/orange lines: $T_{\text{ICB}} = 5700$ K; blue/turquoise lines: $T_{\text{ICB}} = 5500$ K. (For interpretation of the references to colour in this figure legend, the reader is referred to the web version of this article.)

Table 1

Pressure (P), temperature (T), electrical conductivity (σ), thermal conductivity (k) and Lorenz parameter (L) for pure solid iron on the three different adiabats at a temperature of 6350, 5700 and 5500 K respectively.

P (GPa)	T (K)	σ ($10^6 \Omega^{-1} \text{m}^{-1}$)	k ($\text{W m}^{-1} \text{K}^{-1}$)	L ($10^{-8} \text{W} \Omega \text{K}^{-2}$)
329	6350	1.757(6)	313(1)	2.81(2)
365	6350	1.850(8)	330(2)	2.81(2)
329	5700	1.855(8)	294(1)	2.78(2)
364	5700	1.953(10)	307(1)	2.76(2)
329	5500	1.883(8)	286(1)	2.76(2)
364	5500	1.971(11)	297(2)	2.74(2)

carry more heat. The increase of k with temperature is clearly apparent in Fig. 1, both for the liquid and for the solid. In the solid case the increase of k is mitigated by the decrease of σ with T , but it is increased even more by the larger value of L , which varies in the range $2.74\text{--}2.81 \times 10^{-8} \text{W} \Omega \text{K}^{-2}$, as opposed to the values in the liquid where it ranges between 2.48 and $2.51 \times 10^{-8} \text{W} \Omega \text{K}^{-2}$ (Pozzo et al., 2013). The net result is an increase of k by $\sim 27\text{--}33\%$ from the liquid to the solid, an even larger amount than the increase of σ .

3.2. Iron–silicon mixtures

For the iron–silicon mixtures the simulations present an additional degree of complication. Diffusion in the solid occurs at a rate that is far too low to be captured by molecular dynamics methods; therefore, at variance with the liquid case, it is not possible to rely only on MD to generate the relevant ionic positions in configuration space. A typical ionic distribution must be decided at the outset of the MD calculations, which will then be used to sample the high temperature vibrations.

In order to decide how to distribute the silicon atoms in the solid mixtures, we used the results obtained in Alfè et al. (2002). In that work, it was found that when two silicon atoms sit on nearest neighbours sites the free energy of the system increases

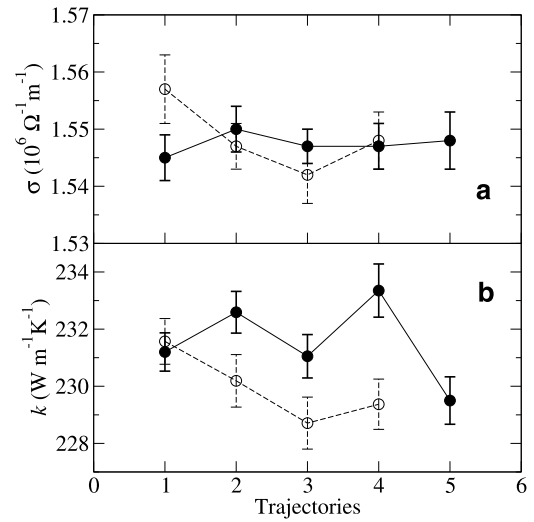


Fig. 2. Electrical conductivity, σ (a), and thermal conductivity, k (b), of 5 statistically independent configurations extracted from a Monte Carlo simulation (filled circles). Also shown 4 trajectories in which Si atoms were distributed entirely at random (open circles). Statistical errors are one standard deviation computed by the scattering of the data. See text for more details.

Table 2

Pressure (P), temperature (T), electrical conductivity (σ), thermal conductivity (k) and Lorenz parameter (L) for the two iron–silicon mixtures, $\text{Fe}_{0.92}\text{Si}_{0.08}$ and $\text{Fe}_{0.93}\text{Si}_{0.07}$, on the two constant adiabats at temperatures of 5700 and 5500 K respectively.

P (GPa)	T (K)	σ ($10^6 \Omega^{-1} \text{m}^{-1}$)	k ($\text{W m}^{-1} \text{K}^{-1}$)	L ($10^{-8} \text{W} \Omega \text{K}^{-2}$)
327	5700	1.505(5)	232(1)	2.70(2)
365	5700	1.540(6)	237(1)	2.70(2)
331	5500	1.547(6)	233(1)	2.74(2)
363	5500	1.595(7)	236(1)	2.70(2)

by ~ 0.25 eV. This value is small when compared to the thermal energy available to each atom in the system; nevertheless it discourages nearest-neighbour occupancy to some extent. Using this value, we performed a Monte Carlo simulation on the lattice in order to find the equilibrium distribution of silicon atoms in the system. From this simulation we extracted 5 statistically independent configurations, and for each of these configurations we performed molecular dynamics simulations of 10 ps in length, from which we extracted 24 configurations (120 configurations in total). These calculations were performed at $p = 331$ GPa and $T = 5500$ K. Results of the electrical and thermal conductivities for these 5 trajectories are displayed in Fig. 2. Statistical errors are represented with one standard deviation, computed by the scattering of data. It is clear that within statistical errors the conductivities computed on the 5 trajectories are almost all equal. To investigate the effect on the conductivities of the exact distribution of the silicon atom in the solid matrix we also produced 4 additional trajectories in which the distribution of the silicon atoms was entirely random. The conductivities obtained from these trajectories are also displayed in Fig. 2, and it is clear that there is no significant difference from those obtained from the previous set of trajectories. For all other thermodynamic states, therefore, we only considered one single trajectory, in which the distribution of the Si atoms was obtained from a Monte Carlo simulation as described above.

In Fig. 3 we show the electrical and thermal conductivities of the two iron–silicon mixtures, $\text{Fe}_{0.92}\text{Si}_{0.08}$ and $\text{Fe}_{0.93}\text{Si}_{0.07}$, at the two corresponding temperatures, 5700 and 5500 K, respectively (see results in Table 2). We also report on the same figure the conductivities of the liquid mixtures $\text{Fe}_{0.82}\text{Si}_{0.10}\text{O}_{0.08}$ and liq-

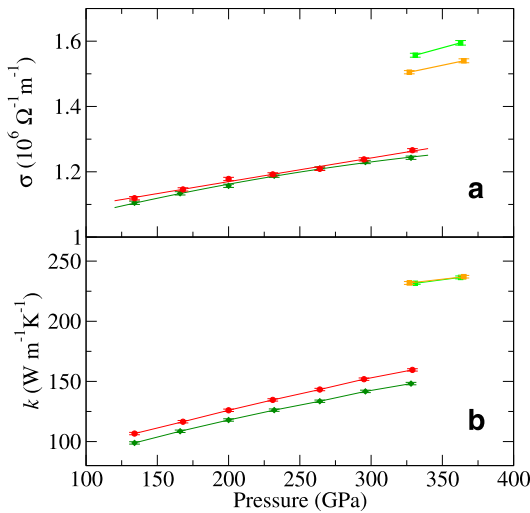


Fig. 3. Electrical conductivity, σ (a), and electronic component of the thermal conductivity, k (b), of liquid $\text{Fe}_{0.82}\text{Si}_{0.10}\text{O}_{0.08}$ (red) and $\text{Fe}_{0.79}\text{Si}_{0.08}\text{O}_{0.13}$ (green) mixtures and solid $\text{Fe}_{0.92}\text{Si}_{0.08}$ (orange) and $\text{Fe}_{0.93}\text{Si}_{0.07}$ (light green) mixtures on the adiabats corresponding to $T_{\text{ICB}} = 5700$ K and $T_{\text{ICB}} = 5500$ K. (For interpretation of the references to colour in this figure legend, the reader is referred to the web version of this article.)

liquid $\text{Fe}_{0.79}\text{Si}_{0.08}\text{O}_{0.13}$ in thermodynamic equilibrium with the solid mixtures. In this case the increase in conductivity from the liquid to the solid is larger than in the pure iron case, which is mainly due to the fact that there is no oxygen in the solid and a slightly lower concentration of silicon. The values for the electrical and thermal conductivities in the solid mixtures are in the range $1.5\text{--}1.6 \times 10^6 \Omega^{-1} \text{m}^{-1}$ and $232\text{--}237 \text{W m}^{-1} \text{K}^{-1}$, respectively, with the low/high values corresponding to ICB/Earth's center pressure–temperature conditions. These values are respectively $\sim 18\text{--}25\%$ and $\sim 45\text{--}56\%$ higher than the corresponding conductivities for the liquid silicon–oxygen–iron mixtures (Pozzo et al., 2013). The Lorenz parameter is almost constant and equal to $2.70\text{--}2.74 \times 10^{-8} \text{W} \Omega \text{K}^{-2}$, which is larger than the value found in the liquid outer core, where it ranges between 2.17 and $2.23 \times 10^{-8} \text{W} \Omega \text{K}^{-2}$ (Pozzo et al., 2013).

The results of our calculations for the two iron–silicon mixtures are larger than the value of $1.2 \times 10^6 \Omega^{-1} \text{m}^{-1}$ measured by Matasov (1977) in an iron sample with an 8% concentration of Si at about 140 GPa and 2700 K. Our results confirm the fact that the conductivity of FeSi solid is smaller than the conductivity of Fe solid, as previously found by Gomi et al. (2010) in a diamond–anvil cell experiment up to 70 GPa at room temperature.

4. Implications for the Earth

These conductivity estimates are significantly higher than those used to date for studies of convection and magnetic field evolution in the inner core (typical values used in literature are $k = 60 \text{W m}^{-1} \text{K}^{-1}$ and $\sigma = 0.5 \times 10^6 \Omega^{-1} \text{m}^{-1}$ with corresponding diffusivities $\kappa = 6.6 \times 10^{-6} \text{m}^2 \text{s}^{-1}$ and $\eta = 1.6 \text{m}^2 \text{s}^{-1}$). The new values are $k = 235 \text{W m}^{-1} \text{K}^{-1}$ and $\sigma = 1.55 \times 10^6 \Omega^{-1} \text{m}^{-1}$ with diffusivities $\kappa = 2.53 \times 10^{-5} \text{m}^2 \text{s}^{-1}$ and $\eta = 0.512 \text{m}^2 \text{s}^{-1}$. The new thermal diffusivity is larger by a factor of 3.83; the new magnetic diffusivity is smaller by a factor of 3.1.

In the liquid core the magnetic field changes mainly by induction of moving fluid; the relevant time scale is the advection time d/v , where d and v are typical length and velocity scales. It takes only a few hundred years for fluid to cross the liquid core at a typical speed of 0.5m s^{-1} . In the inner core the magnetic field can only change by diffusion. The magnetic diffusivity determines the magnetic diffusion time and the relevant time scale is $t_\eta = r_{\text{ic}}^2/\eta$,

where r_{ic} is the radius of the inner core. For $r_{\text{ic}} = 1221$ km, the magnetic diffusion time is $t_\eta = 92$ kyr. There is a large geometrical factor (π^2 for the slowest decaying mode, a dipole field varying radially as a spherical Bessel function) reducing the e-folding time to 10 kyr, but this is still an order of magnitude longer than the advection time in the outer core. We can therefore expect large scale magnetic fields to remain stable in the inner core for thousands of years. Whether or not it can influence the stability of the whole geomagnetic field is a subtle question, since rapid variations do not penetrate a good conductor. One study comparing the effects of insulating and perfectly conducting inner cores found little or no effect (Busse and Simitev, 2008) but, as with all these studies, it had a limited parameter range and more work is needed. Further calculations are needed to explore the role of the inner core in stabilising the geodynamo.

The discontinuity of electrical conductivity at the ICB is small but could produce interesting effects akin to shearing of magnetic field. It might even affect the dynamo action and the morphology of the geomagnetic field.

Our high estimate of thermal conductivity means heat will leak out of the inner core by conduction, making thermal convection less likely. In the extreme case of zero conductivity the temperature within the inner core remains frozen at the melting temperature, $T_m(r)$, appropriate for the pressure at radius r . This must be above the adiabatic gradient for the inner core to undergo thermal convection. In the other extreme case, where conduction is very high, all heat leaks away rapidly to leave an isothermal inner core that will not convect. The thermal diffusion time is $t_\kappa = r_{\text{ic}}^2/\kappa \approx 1.9$ Gyr. The age of the inner core is uncertain, but a value of 1 Gyr (Labrosse et al., 2001) is commonly quoted. Hence we have an intermediate case with temperature gradient below the melting gradient but still allowing the possibility of thermal convection.

Thermal convection at the present day requires that the heat released by cooling, q_s , exceeds conduction down the adiabat, q_a (assuming no radiogenic elements in the inner core). The total heat conducted down the adiabat is

$$q_a = -4\pi r_{\text{ic}}^2 k \frac{dT_a}{dr}, \quad (1)$$

where

$$\frac{dT_a}{dr} = -\frac{dT_a}{dP} \rho_i g_i r \quad (2)$$

is the radial gradient of the adiabatic temperature $T_a(r)$. Here $g = g_i r$ is the acceleration due to gravity, which is taken to vary linearly with radius, and P is the pressure, which is approximately hydrostatic, $dP/dr = \rho_i g_i r$. The density varies little across the inner core so we use a constant $\rho_i = 12700 \text{kg m}^{-3}$.

If the inner core is convecting the temperature will be close to adiabatic. The specific heat of cooling is then (Gubbins et al., 2003)

$$q_s = -\int \rho c_p \frac{DT_a}{Dt} dV_{\text{ic}} \approx -\frac{4\pi r_{\text{ic}}^3}{3} \rho_i c_p \frac{T_i}{T_0} \frac{dT_0}{dt}, \quad (3)$$

where $c_p = 728 \text{J kg}^{-1} \text{K}^{-1}$ is the specific heat capacity at constant pressure, T_i is the temperature at the ICB, $T_0 = 4040$ K the temperature at the core–mantle boundary (CMB) and dT_0/dt the cooling rate at the CMB. We have assumed that T_a varies slowly in time (Gubbins et al., 2003) and neglected a small term in the second step in (3).

Using a rapid cooling rate of $dT_0/dt = 100 \text{K Gyr}^{-1}$ gives $q_a = 1.6$ TW and $q_s = 0.3$ TW, very subcritical. To get $q_s = q_a$ requires that $dT_0/dt \approx 540 \text{K Gyr}^{-1}$, equivalent to a CMB heat-flux $Q = 66$ TW using the core energetics model in Pozzo et al. (2012) (see Gubbins et al., 2003, 2004 for a complete description). Estimates of Q range between 6 and 14 TW (Nimmo, 2007) and so

this calculation suggests the inner core is not presently undergoing thermal convection. This conclusion was also reached by Yukutake (1998).

However, thermal convection might still have been possible earlier in Earth's history (Buffett, 2009; Deguen and Cardin, 2011). To investigate this possibility we use the formulation of Buffett (2009), which ignores the effects of latent heat and gravitational energy release on freezing. This assumption is justified for small inner core radius and provides an elegant solution of the thermal conduction problem in which the temperature gradient takes the form

$$\frac{dT}{dr} = -\rho_i g_i \frac{dT_m}{dP} \frac{1}{(1 + 6t_{ic}/t_\kappa)} r, \quad (4)$$

where t_{ic} is the age of the inner core: conduction reduces the melting gradient by the constant factor $1/(1 + 6t_{ic}/t_\kappa)$, about 1/3 for Buffett's preferred inner core age of 0.6 Gyr (corresponding to $Q = 6$ TW of heat loss from the whole core) and closer to 1/4 if we take $t_{ic} = 1$ Gyr. The pressure derivatives of T_m and T_a vary little in the inner core and we use constant values below. From (2) and (4) it is clear that both adiabatic and melting gradients vary linearly with r ; the temperatures themselves are quadratic in r .

The inner core is thermally unstable at early times if the temperature gradient dT/dr in (4) exceeds the adiabatic gradient. Using our own values for the adiabatic and melting gradients, obtained from *ab initio* calculations, $dT_m/dP = 8.9$ KGPa⁻¹ and $dT_a/dP = 6.7$ KGPa⁻¹, we find the inner core to be subadiabatic at early times for the CMB heat-flux $Q = 6$ TW used by Buffett (2009):

$$T'(r) \approx -1.35 \times 10^{-10} r; \quad T'_a(r) \approx -3.09 \times 10^{-10} r.$$

In this model the condition of neutral stability, given by $dT/dr = dT_a/dr$, is satisfied for a CMB heat-flux $Q = 36$ TW, a very high value. This value exceeds the 5 TW obtained by Buffett (2009) because of our higher values for k and dT_a/dP . Accounting for latent heat release and gravitational energy slows core cooling, making it even harder to drive thermal convection. If correct, this result means the inner core was never thermally unstable, unless a very high CMB heat-flux could be sustained around the time of inner core formation.

Compositional effects may still allow the inner core to convect because less light element partitions into the solid over time (Gubbins et al., 2013). The density gradients arising from thermal and compositional effects are comparable for a CMB heat-flux $Q = 20$ TW, a reasonable value when the inner core was young (Nimmo, 2007). Furthermore, even if the net density gradient is stabilising a doubly-diffusive instability will arise, admittedly on the long thermal diffusion timescale, if (Turner, 1973)

$$\frac{dc}{dr} < \frac{\kappa_c}{\kappa} \frac{\alpha_T}{\alpha_c} \left(\frac{dT_a}{dr} - \frac{dT}{dr} \right), \quad (5)$$

where κ_c is the compositional diffusivity. This condition is always likely to be met because $\kappa_c/\kappa \ll 1$ in the solid.

5. Conclusions

We have studied the electrical and thermal conductivity of pure iron and two iron–silicon solid solutions matching the seismically-determined inner-core boundary density jump at the conditions of Earth's inner core. At the inner core boundary (centre of the Earth) we find thermal and electrical conductivity values of $k = 232$ (237) W m⁻¹ K⁻¹ and $\sigma = 1.5$ (1.6) $\times 10^6$ Ω^{-1} m⁻¹. These values are respectively about 45–56% and 18–25% higher than the corresponding conductivities in the liquid outer core, due to the

fact that the inner core is solid and has a lower concentration of light impurities than the liquid outer core.

The electrical conductivity is higher than any values considered before; it may produce new effects on the geomagnetic field and the geodynamo. Furthermore, there is a discontinuity in conductivity between the bottom of the liquid outer core and the solid inner core, which may also produce some interesting effects. The diffusion time in the inner core is ~ 10 kyr, an order of magnitude longer than the advection time in the liquid core and, for example, the time it takes a polarity reversal to complete. The inner core may be stabilising the geomagnetic field, in part controlling the frequency of reversals.

The thermal conductivity is almost 4 times higher than the highest values currently in use, making the thermal diffusion time comparable to estimates of the inner core age. Heat will leak out as the inner core grows, bringing the temperature towards isothermal. A simple calculation appropriate to the early Earth shows the inner core to be thermally stable unless a core–mantle boundary heat-flux 3–5 times higher than present-day estimates could be sustained at this time. Such high heat-fluxes require rapid core cooling and are not favoured on energetic grounds. Even more heat is needed to maintain inner core convection in recent times, which is very unlikely. These calculations suggest that thermal inner core convection was unlikely, even at early times.

Compositional effects may still make the inner core convect. As the inner core grows the liquid becomes enriched with light elements and further freezing will deposit a lighter solid on the surface of the inner core, producing a stable gradient, but at the same time the partitioning coefficient decreases because of the falling temperature, causing a larger destabilising gradient (Gubbins et al., 2013). The destabilising density gradient due to composition is comparable in magnitude with the stabilising density gradient due to temperature; our numbers favour a convective instability driven by composition but also allow for doubly-diffusive instability with a stable thermal gradient and unstable compositional gradient. Such instabilities could explain the complex seismic structure of the inner core.

Acknowledgements

The work of M.P. was supported by a NERC grant number NE/H02462X/1. Calculations were performed on the HECToR service in the U.K. and also on Legion@UCL as provided by research computing. C.D. is supported by a Natural Environment Research Council personal fellowship, NE/H01571X/1.

References

- Alfè, D., 1999. *Ab initio* molecular dynamics, a simple algorithm for charge extrapolation. *Comput. Phys. Commun.* 118, 31–33.
- Alfè, D., 2009. Temperature of the inner-core boundary of the Earth: Melting of iron at high pressure from first-principles coexistence simulations. *Phys. Rev. B* 79, 060101.
- Alfè, D., Price, G.D., Gillan, M.J., 2002. Iron under Earth's core conditions: Liquid-state thermodynamics and high-pressure melting curve from *ab initio* calculations. *Phys. Rev. B* 65, 165118.
- Alfè, D., Gillan, M.J., Price, G.D., 2007. Temperature and composition of the Earth's core. *Contemp. Phys.* 48, 63–80.
- Alfè, D., Pozzo, M., Desjarlais, M.P., 2012. Lattice electrical resistivity of magnetic bcc iron from first-principles calculations. *Phys. Rev. B* 85, 024102.
- Andersen, H.C., 1980. Molecular-dynamics simulations at constant pressure and/or temperature. *J. Chem. Phys.* 72, 2384–2393.
- Anzellini, S., Dewaele, A., Mezouar, M., Loubeyre, P., Morard, G., 2013. Melting of iron at Earth's inner core boundary based on fast X-ray diffraction. *Science* 340, 464–466.
- Blöchl, P.E., 1994. Projector augmented-wave method. *Phys. Rev. B* 50, 17953–17979.
- Buffett, B.A., 2009. Onset and orientation of convection in the inner core. *Geophys. J. Int.* 179, 711–719.
- Busse, F.H., Simitev, R.D., 2008. Toroidal flux oscillation as possible cause of geomagnetic excursions and reversals. *Phys. Earth Planet. Inter.* 168, 237–243.

- Deguen, R., Cardin, P., 2011. Thermochemical convection in Earth's inner core. *Geophys. J. Int.* 187, 1101–1118.
- Deng, L., Seagle, C., Fei, Y., Shahar, A., 2013. High pressure and temperature electrical resistivity of iron and implications for planetary cores. *Geophys. Res. Lett.* 40, 33–37.
- Desjarlais, M.P., Kress, J.D., Collins, L.A., 2002. Electrical conductivity for warm, dense aluminum plasmas and liquids. *Phys. Rev. E* 66, 025401.
- Dharmaraj, G., Stanley, S., 2012. Effect of inner core conductivity on planetary dynamo models. *Phys. Earth Planet. Inter.* 212–213, 1–9.
- Glatzmaier, G.A., Roberts, P.H., 1995. A 3-dimensional convective dynamo solution with rotating and finitely conducting inner-core and mantle. *Phys. Earth Planet. Inter.* 91, 63–75.
- Gomi, H., Ohta, K., Hirose, K., 2010. Electrical conductivity measurement of iron at high static pressure. In: Fall Meeting. 13–17 December, 2010. AGU, San Francisco, California. Abstract #MR23A-2012.
- Gomi, H., Ohta, K., Hirose, K., Labrosse, S., Caracas, R., Verstraete, M.J., Hernlund, J., 2013. The high conductivity of iron and thermal evolution of the Earth's core. *Phys. Earth Planet. Inter.* 224, 88–103.
- Gubbins, D., 1999. The distinction between geomagnetic excursions and reversals. *Geophys. J. Int.* 137, F1–F3.
- Gubbins, D., Alfè, D., Masters, T.G., Price, D., Gillan, M.J., 2003. Can the Earth's dynamo run on heat alone?. *Geophys. J. Int.* 155, 609–622.
- Gubbins, D., Alfè, D., Masters, T.G., Price, D., 2004. Gross thermodynamics of two-component core convection. *Geophys. J. Int.* 157, 1407–1414.
- Gubbins, D., Alfè, D., Davies, C., 2013. Compositional instability of Earth's solid inner core. *Geophys. Res. Lett.* 40, 1084–1088.
- Gunnarsson, O., Calandra, M., Han, J.E., 2003. Colloquium: saturation of electrical resistivity. *Rev. Mod. Phys.* 75, 1085–1099.
- Hollerbach, R., Jones, C.A., 1993. A geodynamo model incorporating a finitely conducting inner core. *Phys. Earth Planet. Inter.* 75, 317–327.
- Ishii, M., Dziewonski, A.M., 2002. The innermost inner core of the earth: Evidence for a change in anisotropic behavior at the radius of about 300 km. *Proc. Natl. Acad. Sci. USA* 99, 14026–14030.
- Jeanloz, R., Wenk, H.R., 1988. Convection and anisotropy of the inner core. *Geophys. Res. Lett.* 15, 72–75.
- Konôpková, Z., Lazor, P., Goncharov, A.F., Struzhkin, V.V., 2011. Thermal conductivity of hcp iron at high pressure and temperature. *High Press. Res.* 31, 228–236.
- Kresse, G., Furthmüller, J., 1996. Efficiency of ab-initio total energy calculations for metals and semiconductors using a plane-wave basis set. *Comput. Mater. Sci.* 6, 15–50.
- Kresse, G., Joubert, D., 1999. From ultrasoft pseudopotentials to the projector augmented-wave method. *Phys. Rev. B* 59, 1758–1775.
- Labrosse, S., Poirier, J.-P., Le Moëul, J.-L., 2001. The age of the inner core. *Earth Planet. Sci. Lett.* 190, 111–123.
- Laj, C., Channel, J.E.T., 2007. Geomagnetic excursions. In: Schubert, G. (Ed.), *Treatise on Geophysics*, vol. 5. Elsevier, Amsterdam, pp. 373–416.
- Matassov, G., 1977. The electrical conductivity of iron–silicon alloys at high pressure and the Earth's core. PhD thesis. University of California.
- Nimmo, F., 2007. Thermal and compositional evolution of the core. In: Schubert, G. (Ed.), *Treatise on Geophysics*, vol. 9. Elsevier, Amsterdam, pp. 217–242.
- Perdew, J.P., Chevary, J.A., Vosko, S.H., Jackson, K.A., Pederson, M.R., Singh, D.J., Fiolhais, C., 1992. Atoms, molecules, solids, and surfaces – Applications of the generalized gradient approximation for exchange and correlation. *Phys. Rev. B* 46, 6671–6687.
- Poirier, J.P., 1994. Light-elements in the Earth's outer core – a critical review. *Phys. Earth Planet. Inter.* 85, 319–337.
- Pozzo, M., Davies, C., Gubbins, D., Alfè, D., 2012. Thermal and electrical conductivity of iron at Earth's core conditions. *Nature* 485, 355–358.
- Pozzo, M., Davies, C., Gubbins, D., Alfè, D., 2013. Transport properties for liquid silicon–oxygen–iron mixtures at Earth's core conditions. *Phys. Rev. B* 87, 014110.
- Sha, X., Cohen, R.E., 2011. First-principles studies of electrical resistivity of iron under pressure. *J. Phys. Condens. Matter* 23, 075401.
- Tromp, J., 2001. Inner-core anisotropy and rotation. *Annu. Rev. Earth Planet. Sci.* 29, 47–69.
- Turner, J.S., 1973. *Buoyancy Effects in Fluids*. Cambridge University Press.
- Wang, Y., Perdew, J.P., 1991. Correlation hole of the spin-polarized electron-gas, with exact small-wave-vector and high-density. *Phys. Rev. B* 44, 13298–13307.
- Wicht, J., 2002. Inner-core conductivity in numerical dynamo simulations. *Phys. Earth Planet. Inter.* 132, 281–302.
- Wiedemann, D., Franz, R., 1853. Ueber die Wärme-Leitungsfähigkeit der Metalle. *Ann. Phys.* 89, 497–531.
- Yukutake, T., 1998. Implausibility of thermal convection in the Earth's solid inner core. *Phys. Earth Planet. Inter.* 108, 1–13.